Available online at www.sciencedirect.com
ScienceDirect
Comput. Methods Appl. Mech. Engrg. 414 (2023) 116159
Computer methods in applied mechanics and engineering
www.elsevier.com/locate/cma

An arbitrarily Lagrangian–Eulerian SPH scheme with implicit iterative particle shifting procedure

P. Rastelli[a], R. Vacondio[a,*], J.C. Marongiu[b]

[a] *Department of Engineering and Architecture, University of Parma, Parma, Italy*
[b] *R&D Department, ANDRITZ Hydro, Vevey, Switzerland*

Received 9 March 2023; received in revised form 2 May 2023; accepted 28 May 2023
Available online 19 June 2023

Abstract

This work presents an Arbitrarily Lagrangian–Eulerian Smoothed Particle Hydrodynamics (ALE-SPH) scheme for Navier–Stokes equations where the particle distribution is optimized by an Implicit Iterative Particle Shifting (IIPS) correction capable of improving the accuracy of the SPH spatial operators. Here two different possible approaches, based respectively on Moving Least Square (MLS) and on convective fluxes have been adopted to embed the IIPS formulation in an ALE-SPH scheme. The theoretical second-order convergence rate has been achieved for the Taylor–Green flow at Reynolds number $Re = 100$. Results obtained with the proposed numerical scheme for the Moving box and the Impinging jet test cases confirm that the accuracy is significantly improved, with respect to existing quasi-Lagrangian ALE-SPH schemes.

Keywords: Navier–Stokes equations; SPH; Smoothed Particle Hydrodynamics; Shifting

1. Introduction

The SPH models have been first developed for astrophysical studies by Gingold and Monaghan [1] and by Lucy [2], later, these methods have been extended to solve fluid dynamics problems by Monaghan [3,4]. The SPH schemes are meshless methods, in which the computational domain is discretized by moving interpolation points called also fluid particles. Due to the Lagrangian nature of SPH schemes, the fluid particles inherently follow the streamlines, making these methods suitable for describing applications with free surfaces [5–7] highly fragmented flows [8], complex fluid–structure interactions [9,10] and multi-fluid interfaces [11–13]. However, as a relevant drawback, the Lagrangian nature introduces not uniform particles distribution which might reduce the accuracy of the scheme. The relations between the particle isotropy and the accuracy of the SPH spatial interpolation have been investigated by Quinlan et al. [14], demonstrating that the theoretical second-order of convergence of the SPH scheme, at continuous level, can be restored at discrete level, exclusively whether the particle distribution is homogeneous. In order to reduce the particle anisotropy, different regularization methodologies, such as XSPH [15], remeshing techniques, or reinitialization algorithms [16], have been initially proposed for SPH schemes. The so-called Particle Shifting Techniques (PSTs), originally proposed by Nestor et al. [17] within the framework of Finite

* Corresponding author.
E-mail address: renato.vacondio@unipr.it (R. Vacondio).

https://doi.org/10.1016/j.cma.2023.116159
0045-7825/

Volume Particle Method (FVPM), was very effective in improving the stability and accuracy of Incompressible SPH (ISPH) schemes [18–20]. The shifting technique has been applied also in Weakly Compressible SPH (WCSPH) schemes, [21–24] or in the ALE formulation, firstly proposed in [25], in which the shifting correction is applied to the transport velocity [26–28] maintaining the consistency of the numerical scheme. Recently Michel et al. [29], presented a review of different explicit particle shifting formulations available in literature, analysing their properties in terms of invariance and accuracy and proposing an enhanced approach. Regardless of the properties of the numerical scheme adopted, in the above-mentioned shifting formulations, the shifting displacements are generally computed using a time-explicit approximation of Fick's diffusion law, computing the particles concentration gradients using the particles position at the previous time step. This approach has been demonstrated to be effective for specific applications, however, a desired level of particles distribution isotropy cannot be guaranteed. To overcome this limitation, recently, Rastelli et al. [30] introduced the Implicit Iterative Particle Shifting (IIPS) methodology, based on a minimization procedure for the gradient of particles concentration, to maintain the discretization error under a threshold level in the whole domain. The IIPS procedure proposed in [30] is a purely geometric modification of particles position, without distinct concerns regarding the consistency of the physical quantities attached to the particles and to the properties of the adopted numerical scheme. In the present work the IIPS algorithm is embedded in the ALE-SPH scheme called ASPHODEL [27,31,32] proposing two different strategies. The first one is based on an Advection Correction Step (ACS) introduced in the formulation to update the physical quantities. The second strategy is a second-order MLS reinterpolation, to update the physical quantities from the old to the new particle distribution.

This paper is organized as follows, in Section 2 the governing equation for fluid dynamic expressed in the ALE-SPH formalism are reported, then, in Section 3 the particle shifting techniques and, in particular, the implicit particle shifting are briefly recalled. Later in Section 4 the innovative methodology used to introduce the IIPS technique in the ALE-SPH scheme is explained, and in Section 5 the proposed numerical scheme is validated against two different applications.

2. Methodology

2.1. Governing equations for ALE-SPH models

In this work, the governing equations of fluids are presented as a system of partial differential equations; in its Lagrangian form the equations for conservation of mass and momentum are,

$$\begin{aligned} \frac{d\rho}{dt} &= -\rho \nabla \cdot \boldsymbol{v} \\ \frac{d\boldsymbol{v}}{dt} &= -\frac{1}{\rho}\nabla p + \nu \nabla^2 \boldsymbol{v} + \boldsymbol{g} \end{aligned} \tag{1}$$

where ρ and $\boldsymbol{v}$ are respectively the density and the velocity of the fluid, p is the pressure field, ν the kinematic viscosity and the gravity force is $\boldsymbol{g}$. The SPH methods have been firstly used to discretize the set of equations for fluid dynamics through the original formalism introduced by Monaghan [3]. To solve the system, a weakly-compressible approach can be adopted and an equation of state is needed to couple Eqs. (1). Specifically, we adopted the barotropic Tait's equation [5]:

$$p = \frac{c_0^2 \rho_0}{\gamma}\left[\left(\frac{\rho}{\rho_0}\right)^{\gamma} - 1\right] + p_0, \tag{2}$$

where $\gamma = 7$ is the polytropic fluid coefficient and c_0, ρ_0 and p_0 are respectively the reference speed of sound, the reference density and the reference pressure.

Following the nature of the meshless methods the computational domain is split into discrete points, to derive the SPH governing equations. The fluid particles are material points that move in time and space carrying the physical quantities. Among many formalisms introduced in SPH, the present work adopts a weakly-compressible ALE scheme [25] which is able to generalize both the Eulerian and the Lagrangian description of fluids, [33], by defining the arbitrary transport velocity $\boldsymbol{v}_0$.

The numerical scheme developed in [27,31,32,34], which has been used to validate the methodologies illustrated in the following sections, presents the governing equations, written in the discrete ALE-SPH formulations, in the following form,

$$\begin{cases} \dfrac{d\mathbf{x}_i}{dt} = \boldsymbol{v}_{0i} \\ \dfrac{d\omega_i}{dt} = \omega_i \displaystyle\sum_{j=1}^{J} 2\left(\boldsymbol{v}_0(\mathbf{x}_{ij}) - \boldsymbol{v}_{0i}\right) \nabla W_{ij}\omega_j \\ \dfrac{d\omega_i\rho_i}{dt} = -\omega_i \displaystyle\sum_{j=1}^{J} 2\rho_{ij}^E \left(\boldsymbol{v}_{ij}^E - \boldsymbol{v}_0(\mathbf{x}_{ij})\right) \nabla W_{ij}\omega_j \\ \dfrac{d\omega_i\rho_i\boldsymbol{v}_i}{dt} = -\omega_i \displaystyle\sum_{j=1}^{J} 2\left[\rho_{ij}^E \boldsymbol{v}_{ij}^E \otimes \left(\boldsymbol{v}_{ij}^E - \boldsymbol{v}_0(\mathbf{x}_{ij})\right) + p_{ij}^E\right] \nabla W_{ij}\omega_j + \omega_i\rho_i\boldsymbol{g} \end{cases} \tag{3}$$

where i represents the calculation point, with the associated volume ω_i, whereas J indicate the total number of surrounding particles, among them, j denotes a generic neighbour with the relative volume ω_j. ρ_{ij}^E, ρ_{ij}^E, $\boldsymbol{v}_{ij}^E$, are the solution of a Riemann problem, computed at the interface between particle i and j and the particles interface velocity is defined as $\boldsymbol{v}_0(\mathbf{x}_{ij}) = \frac{\boldsymbol{v}_{0i}+\boldsymbol{v}_{0j}}{2}$. The Monotone Upstream-centred Scheme for Conservation Laws (MUSCL) second-order method is adopted to reconstruct the Left and Right state, $\boldsymbol{\Phi}_L$ and $\boldsymbol{\Phi}_R$, of the Reimann problem, [35]. Moreover, Eqs. (3) are updated in time by means of explicit Runge–Kutta (RK) formulation [36].

3. Particle shifting technique

It is well known that one of the issue of SPH schemes is the low convergence rate [37], the particles distribution influences the accuracy of the SPH spatial interpolation [14,38]. For this reason, Particles Shifting Techniques (PSTs) have been introduced in the past, aiming at preventing strong particle anisotropy generated by the Lagrangian motion. As a global view, PSTs are formulated with two different approaches that can be adapted based on the specific solver for the governing equations in which they are implemented. The correction term can be formulated as displacement directly applied to the particle position,

$$\bar{\mathbf{x}}_i = \mathbf{x}_i + \delta\mathbf{x}_i, \tag{4}$$

where $\mathbf{x}_i$ is the original position, $\bar{\mathbf{x}}_i$ is the adjusted or shifted position and $\delta\mathbf{x}_i$ is the shifting vector of the ith particle, [18,19,21,22,24,39]. These techniques have been effective in specific applications in preventing highly non-isotropic particle distributions, however, particles no longer follow the Lagrangian trajectories and advection terms have to be added to prevent inconsistencies [24].

To overcome these issues and taking advantage of the ALE-SPH formalism, Oger et al. [26], Neuhauser [27] and Antuono et al. [40] defined the transport velocity by adding a shifting correction term to the fluid velocity:

$$\boldsymbol{v}_{\mathbf{0}i} = \boldsymbol{v}_i + \delta\boldsymbol{v}_i, \tag{5}$$

leading to a consistent quasi-Lagrangian scheme. The particle shifting techniques are based on Fick's law of diffusion where the correction of the particle position (for WC-SPH) or of the transport velocity (for ALE-SPH) for particle i is proportional to the particles concentration gradient, defined as,

$$\nabla C_i = \sum_{j=1}^{J} \nabla W_{ij}\omega_j, \tag{6}$$

In Eqs. (4) and (5) where an explicit formulation is adopted, the position or transport velocity correction terms are explicitly imposed on the single particle, using only local information. As previously reported, a different approach has been recently proposed in [30], where the shifting correction to the particle position is computed implicitly obtaining a modification of the particles distribution in the entire domain. The implicit shifting is based on the minimization of the concentration gradient components for all particles in the domain. The main steps of the IIPS methodology are briefly recalled here, the reader is referred to [30] for additional details.

Initially, for each component of the particle concentration gradient of the ith particle ∇C_i, the Taylor series expansions truncated at the first order are expressed as,

$$\frac{\partial C_i(\bar{\mathbf{X}},\bar{\mathbf{Y}})}{\partial x} = \frac{\partial C_i(\mathbf{X},\mathbf{Y})}{\partial x} + \sum_{j=1}^{J} \frac{\partial}{\partial x_j}\frac{\partial C_i(\mathbf{X},\mathbf{Y})}{\partial x}(\bar{x}_j - x_j) + \sum_{j=1}^{J} \frac{\partial}{\partial y_j}\frac{\partial C_i(\mathbf{X},\mathbf{Y})}{\partial x}(\bar{y}_j - y_j) + \mathcal{O}((\bar{x}_i - x_i)(\bar{y}_i - y_i))^2, \quad (7)$$

and

$$\frac{\partial C_i(\bar{\mathbf{X}},\bar{\mathbf{Y}})}{\partial y} = \frac{\partial C_i(\mathbf{X},\mathbf{Y})}{\partial y} + \sum_{j=1}^{J} \frac{\partial}{\partial x_j}\frac{\partial C_i(\mathbf{X},\mathbf{Y})}{\partial y}(\bar{x}_j - x_j) + \sum_{j=1}^{J} \frac{\partial}{\partial y_j}\frac{\partial C_i(\mathbf{X},\mathbf{Y})}{\partial y}(\bar{y}_j - y_j) + \mathcal{O}((\bar{x}_i - x_i)(\bar{y}_i - y_i))^2. \quad (8)$$

where $(\mathbf{X},\mathbf{Y})$ and $\left(\bar{\mathbf{X}},\bar{\mathbf{Y}}\right)$ are the vectors of particle coordinates in 2-D for all $i = 1,\ldots,n$ particles used to discretize the computational domain. As previously stated, in order to improve the accuracy of the SPH operator at the discrete level, the particle concentration gradient, ∇C, has to be zero for any particle in the domain. By imposing this condition on Eqs. (7) and (8) and neglecting non-linear terms, it leads to:

$$\sum_{j=1}^{J} \frac{\partial^2 W\left(\left(x_i - x_j\right),\left(y_i - y_k\right)\right)}{\partial x_j^2}\omega_j\left(\bar{x}_j - x_j\right) + \sum_{j=1}^{J} \frac{\partial^2 W\left(\left(x_i - x_j\right),\left(y_i - y_k\right)\right)}{\partial x_j \partial y_j}\omega_j\left(\bar{y}_j - y_j\right) = \frac{\partial C_i(\mathbf{X},\mathbf{Y})}{\partial x}, \quad (9)$$

and

$$\sum_{j=1}^{J} \frac{\partial^2 W\left(\left(x_i - x_j\right),\left(y_i - y_k\right)\right)}{\partial y_j \partial x_j}\omega_j\left(\bar{x}_j - x_j\right) + \sum_{j=1}^{J} \frac{\partial^2 W\left(\left(x_i - x_j\right),\left(y_i - y_k\right)\right)}{\partial y_j^2}\omega_j\left(\bar{y}_j - y_j\right) = \frac{\partial C_i(\mathbf{X},\mathbf{Y})}{\partial y}. \quad (10)$$

Eqs. (9) and (10) are used to assemble a system of linear equations, $\mathbf{Ax} = \mathbf{B}$, where the terms in the known vector, $\mathbf{B}$, represent the particles concentration gradient of the original particle distribution and the terms on the unknown vector $\mathbf{x}$ correspond to the particle shifting $\delta\mathbf{x}_i = \left(\bar{x}_i - x_j\right),\left(\bar{y}_i - y_j\right)$ for $j = 1,\ldots,n$. Due to the linear approximations, the procedure needs to be repeated, details in [30].

While the IIPS procedure is more computationally expensive than the explicit shifting, it is not activated at every timestep but only when the maximum value of the gradient concentration over the whole domain is greater than a pre-defined threshold.

4. Implicit iterative particle shifting in ALE-SPH scheme

Hereafter, methodologies to integrate the IIPS algorithm, described in Section 3, in an SPH-ALE solver are discussed. In particular, we address the issue of updating the physical quantities (volume, density and velocity) attached to the particles in a way that is consistent with the particle motion defined by the implicit shifting formulation.

In the ALE-SPH models proposed in [26,27] an explicit shifting formulation was adopted and the physical quantities were updated consistently by means of Eqs. (3) thanks to the possibility of arbitrarily define the transport velocity $\boldsymbol{v}_0$. However, the shifting correction $\delta\boldsymbol{v}$ has to be maintained small to avoid issues and instability in the numerical scheme and this prevents the possibility of keeping the ∇C small for all particles in the domain at every timestep. Conversely, in the IIPS formulation herein proposed there is no such limitation as the particles positions are adjusted accordingly to the pure geometrical formulation of the IIPS. Following these considerations, two different methodologies to update the physical quantities, are proposed, the first one based on an Advection Correction Step (ACS) and the second one adopt a Moving Least Square re-interpolation.

4.1. IIPS with advection correction step

Following the explicit nature of the ALE-SPH scheme, the displacement obtained from the IIPS is used to compute the transport velocity in an Advection Correction Step (ACS). We underline that during ACS the physical

time of the adopted numerical scheme to solve Eqs. (3) is frozen. Eq. (4), is manipulated as,

$$\bar{\mathbf{x}} = \mathbf{x} + \delta\mathbf{x} \quad \rightarrow \quad \delta\mathbf{x} = \bar{\mathbf{x}} - \mathbf{x} \tag{11}$$

and, isolating the implicit shifting term, an advection correction is applied considering a fictitious time step Δt^*,

$$\frac{\delta\mathbf{x}}{\Delta t^*} = \frac{\bar{\mathbf{x}} - \mathbf{x}}{\Delta t^*} = \boldsymbol{v}_{ACS}, \tag{12}$$

defining the arbitrary transport velocity $\boldsymbol{v}_{ACS}$ for the Advection Correction Step.

Due to the ALE-SPH nature, the interpolation points displacements, obtained through the IIPS procedure, generate convective fluxes that need to be taken into account. To compute the variation of the physical quantities associated with the convective fluxes, the above-mentioned defined $\boldsymbol{v_0}$, Eq. (12), is introduced in the ALE-SPH governing equation [25,26]. Then, neglecting internal or external forces, the set of equations that have to be solved in the advection correction step are rewritten,

$$\begin{cases} \dfrac{\delta\mathbf{x}_i}{\Delta t^*} = \boldsymbol{v}_{ACSi} \\ \dfrac{d\omega_i}{\Delta t^*} = \omega_i \displaystyle\sum_{j=1}^{J} \left(\boldsymbol{v}_{ACSj} - \boldsymbol{v}_{ACSi}\right) \nabla W_{ij}\omega_j \\ \dfrac{d\omega_i\rho_i}{\Delta t^*} = -\omega_i \displaystyle\sum_{j=1}^{J} \left(\rho_i \left(\boldsymbol{v}_{ACSi}\right) + \rho_j \left(\boldsymbol{v}_{ACSj}\right)\right) \nabla W_{ij}\omega_j \\ \dfrac{d\omega_i\rho_i\boldsymbol{v}_i}{\Delta t^*} = -\omega_i \displaystyle\sum_{j=1}^{J} \left(\rho_i\boldsymbol{v}_i \otimes \left(\boldsymbol{v}_{ACSi}\right) + \rho_j\boldsymbol{v}_j \otimes \left(\boldsymbol{v}_{ACSj}\right)\right) \nabla W_{ij}\omega_j \end{cases} \tag{13}$$

The equations in the system (13), which has no relation to the physical time step, need to be solved exclusively after the IIPS procedure. Then, substituting Eq. (12), the ALE-SPH fictitious system is formulated,

$$\begin{cases} \dfrac{\delta\mathbf{x}_i}{\Delta t^*} = \boldsymbol{v}_{0i} \\ \dfrac{d\omega_i}{\Delta t^*} = \omega_i \displaystyle\sum_{j=1}^{J} \left(\dfrac{\delta\mathbf{x}_j}{\Delta t^*} - \dfrac{\delta\mathbf{x}_i}{\Delta t^*}\right) \nabla W_{ij}\omega_j \\ \dfrac{d\omega_i\rho_i}{\Delta t^*} = -\omega_i \displaystyle\sum_{j=1}^{J} \left(\rho_i \left(\dfrac{\delta\mathbf{x}_i}{\Delta t^*}\right) + \rho_j \left(\dfrac{\delta\mathbf{x}_j}{\Delta t^*}\right)\right) \nabla W_{ij}\omega_j \\ \dfrac{d\omega_i\rho_i\boldsymbol{v}_i}{\Delta t^*} = -\omega_i \displaystyle\sum_{j=1}^{J} \left(\rho_i\boldsymbol{v}_i \otimes \left(\dfrac{\delta\mathbf{x}_i}{\Delta t^*}\right) + \rho_j\boldsymbol{v}_j \otimes \left(\dfrac{\delta\mathbf{x}_j}{\Delta t^*}\right)\right) \nabla W_{ij}\omega_j \end{cases} \tag{14}$$

The time step Δt^*, as expected, has no influence and it is cancelled out,

$$\begin{cases} \bar{\mathbf{x}}_i - \mathbf{x}_i = \delta\mathbf{x}_i \\ \bar{\omega}_i - \omega_i = \omega_i \displaystyle\sum_{j=1}^{J} \left(\delta\mathbf{x}_j - \delta\mathbf{x}_i\right) \nabla W_{ij}\omega_j \\ \bar{\omega}_i\bar{\rho}_i - \omega_i\rho_i = -\omega_i \displaystyle\sum_{j=1}^{J} \left(\rho_i \left(\delta\mathbf{x}_i\right) + \rho_j \left(\delta\mathbf{x}_j\right)\right) \nabla W_{ij}\omega_j \\ \bar{\omega}_i\bar{\rho}_i\bar{\boldsymbol{v}}_i - \omega_i\rho_i\boldsymbol{v}_i = -\omega_i \displaystyle\sum_{j=1}^{J} \left(\rho_i\boldsymbol{v}_i \otimes \left(\delta\mathbf{x}_i\right) + \rho_j\boldsymbol{v}_j \otimes \left(\delta\mathbf{x}_j\right)\right) \nabla W_{ij}\omega_j \end{cases} \tag{15}$$

with $\bar{\omega}_i$, $\bar{\rho}_i$, and $\bar{\boldsymbol{v}}_i$ the updated quantities at the end of the Advection Correction Step.

A preliminary consideration regarding the maximum implicit displacement has to be pointed out; the IIPS methodology has no numerical constrains on the maximum allowed shifting, even if the conducted numerical experiences have shown that for low perturbed distributions the values are usually less than 0.2Δ. Nevertheless, it has been proposed to indirectly bound the displacements, reducing the particle displacement with a factor related

to the CFL condition. For this purpose, a numerical coefficient, N, is computed at the end of each implicit procedure as the nearest greater integer number for all particles as follows

$$N = \left\lceil \frac{(\max_i |\delta \mathbf{x}_i|)}{CFL\ \Delta} \right\rceil. \tag{16}$$

where the symbol $\lceil \rceil$ stands for the ceiling function and Δ is the initial particle distance. Therefore, the final version of Eqs. (13) is rewritten as,

$$\begin{cases} \bar{\mathbf{x}}_i - \mathbf{x}_i = \dfrac{\delta \mathbf{x}_i}{N} \\ \bar{\omega}_i - \omega_i = \omega_i \displaystyle\sum_{j=1}^{J} \left(\frac{\delta \mathbf{x}_j}{N} - \frac{\delta \mathbf{x}_i}{N} \right) \nabla W_{ij} \omega_j \\ \bar{\omega}_i \bar{\rho}_i - \omega_i \rho_i = -\omega_i \displaystyle\sum_{j=1}^{J} \left(\rho_i \left(\frac{\delta \mathbf{x}_i}{N} \right) + \rho_j \left(\frac{\delta \mathbf{x}_j}{N} \right) \right) \nabla W_{ij} \omega_j \\ \bar{\omega}_i \bar{\rho}_i \bar{\boldsymbol{v}}_i - \omega_i \rho_i \boldsymbol{v}_i = -\omega_i \displaystyle\sum_{j=1}^{J} \left(\rho_i \boldsymbol{v}_i \otimes \left(\frac{\delta \mathbf{x}_i}{N} \right) + \rho_j \boldsymbol{v}_j \otimes \left(\frac{\delta \mathbf{x}_j}{N} \right) \right) \nabla W_{ij} \omega_j \end{cases} \tag{17}$$

These equations are integrated for N times to obtain the final value of the field quantities in the position obtained using the implicit iterative algorithm. Please note that the RHSs of Eqs. (17) are computed for each of the N sub-steps.

The set of equations proposed is consistent with the ALE-SPH formalism and it conserves mass and momentum for particles in the interior region of fluid.

4.2. IIPS with MLS reconstruction

A second possible approach here proposed is based on the idea of remapping the physical quantities from the particles positions computed at the end of the physical time step $(\mathbf{X}, \mathbf{Y})$ to the ones computed by the IIPS procedure $(\bar{\mathbf{X}}, \bar{\mathbf{Y}})$. This approach has been similarly utilized in explicit iterative particle shifting procedure by Vacondio & Rogers [23]. The spatial interpolation procedure needs to be chosen in such a way that it minimizes the unavoidable numerical diffusivity generated by the reinterpolation. In this work, the second order Moving Least Square (MLS), presented in [41] is adopted and the generic quantity ϕ_i at particle i is obtained by solving the following linear system:

$$\mathbf{M_i}\ \boldsymbol{\Phi_i} = \mathbf{B_i} \tag{18}$$

where the matrix $\mathbf{M_i} = \sum_{j=1}^{J} (\psi_{ij} \otimes \psi_{ij}) W_{ij} \omega_j$, the vector $\mathbf{B_i} = \sum_{j=1}^{J} \phi_j \psi_{ij} W_{ij} \omega_j$ and the vector $\boldsymbol{\Phi_i} = [\phi_i, \nabla \phi_i]$. It has to be underlined that ϕ_i is the generic quantity at the updated particles distribution, $(\bar{\mathbf{X}}, \bar{\mathbf{Y}})$, while ϕ_j is the generic quantities at the original particle distribution $(\mathbf{X}, \mathbf{Y})$. Then, $\boldsymbol{\psi}_{ij} = \left[1, \boldsymbol{\Delta}_x, \boldsymbol{\Delta}_y, \boldsymbol{\Delta}_{xy}, \boldsymbol{\Delta}_x^2, \boldsymbol{\Delta}_y^2\right]$ and $\boldsymbol{\Delta}_x = (x_i - x_j)/h_i$, $\boldsymbol{\Delta}_y = (y_i - y_j)/h_i$, $\boldsymbol{\Delta}_{xy} = (x_i - x_j)(y_i - y_j)/h$.

5. Evaluation of the IIPS in ALE-SPH

In this section the notation "Implicit iterative shifting" stands for no correction of physical quantities (particles position is moved using the IIPS procedure, but the physical quantities are not updated), "Implicit iterative shifting ACS" stands for the procedure presented in Eqs. (17) and "Implicit iterative shifting MLS II" stands for equation methodology in Eq. (18), while "Explicit shifting" is referred to the shifting described in [27] and briefly recalled in Section 3.

In order to evaluate the feasibility of the two methodologies explained in Sections 4.1 and 4.2, they have been initially tested using the two-dimensional Taylor–Green vortex which has an analytical solution for the Navier–Stokes equations and it has been widely simulated in SPH through incompressible [18] and weakly compressible [22] SPH schemes. This test represents a counter-rotating decaying flow, in which the streamlines are highly distorted and it is really demanding if a fully Lagrangian approach is adopted due to the continuous distortion applied to the particles distribution by the analytical velocity field. The domain is defined in a square box with bi-periodic

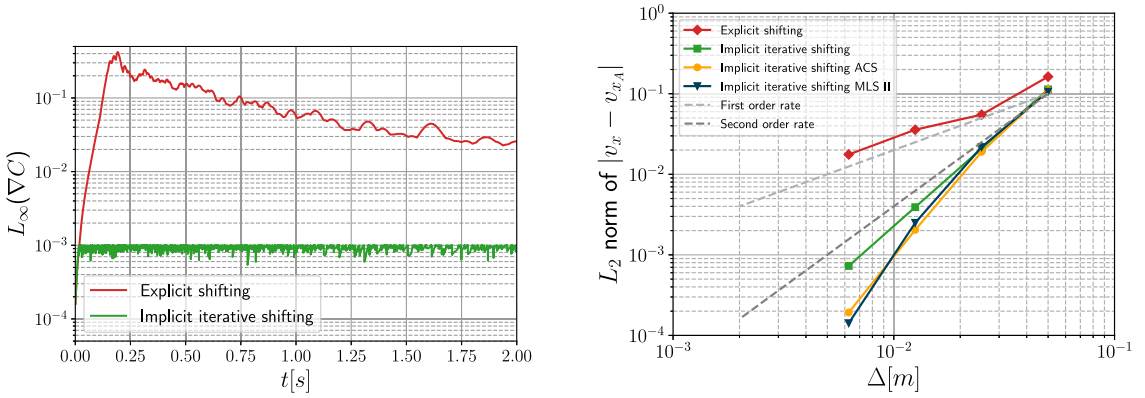

(a) $L_\infty(\nabla C)$ obtained with the IIPS and explicit shifting for $\Delta/L = 0.00625$

(b) Convergence analysis $L_2|\boldsymbol{v}_x - \boldsymbol{v}_{xA}|$, implicit particle shifting comparison at $t = 1s$.

Fig. 1. TGV test case. Particle distribution and convergence analysis, results obtained with $h/\Delta = 2$.

Table 1
TGV test case. Convergence analysis results, $L_2|\boldsymbol{v}_x - \boldsymbol{v}_{xA}|$ and convergence ratio θ, implicit iterative shifting.

	[27]		IIPS		IIPS-ACS		IIPS-MLS II	
Δ/L	$L_2(\boldsymbol{v}_x)$	θ	$L_2(\boldsymbol{v}_x)$	θ	$L_2(\boldsymbol{v}_x)$	θ	$L_2(\boldsymbol{v}_x)$	θ
0.05	0.1628		0.1139		0.1111		0.1062	
0.025	0.0556	1.55	0.0208	2.44	0.0189	2.55	0.0218	2.28
0.0125	0.0337	0.72	0.0039	2.42	0.0020	3.22	0.0025	3.12
0.00625	0.0176	0.93	0.0007	2.41	0.00019	3.41	0.00014	4.13

boundary conditions, the velocity components u and v on x and y directions, respectively and the pressure p are computed as,

$$\begin{cases} u\,(x,\,y) = & Ue^{-8\pi^2 t/Re} cos(2\pi x/L) sin(2\pi y/L) \\ v\,(x,\,y) = & Ue^{-8\pi^2 t/Re} sin(2\pi x/L) cos(2\pi y/L) \\ p\,(x,\,y) = & \dfrac{\rho}{4} e^{-16\pi^2 t/Re} \left[cos(4\pi x/L) + cos(4\pi y/L)\right] \end{cases} \tag{19}$$

where ρ, is the density and $Re = UL/\nu$ is the Reynolds number computed with ν, the kinematic viscosity, U the initial reference velocity and L the characteristic length of the problem. In the numerical experiments presented below, L = 1 m coincides with the size of the domain while U = 1 m/s, and ν = 0.01 m^2/s resulting in Re = 100.

The quality of the particle distribution has been evaluated through the maximum value of the particles concentration gradient $L_\infty(\nabla C)$. The implicit iterative procedure has been applied imposing the threshold $L_\infty(\nabla C)$ = $0.001/h$ as the value that triggers the IIPS correction for the particles distribution where h is the smoothing length of the kernel function. As it can be seen in Fig. 1(a), the IIPS procedure is able to keep the $L_\infty(\nabla C)$ below the pre-defined threshold while the same quantity becomes more than two orders of magnitude larger with the explicit shifting formulation demonstrating that the IIPS is able to significantly improve the quality of the particles distribution. Moreover, a convergence analysis has been done using Δ/L = 0.05, 0.025, 0.0125, 0.00625 in order to assess the effectiveness of the methodologies illustrated in Sections 4.1 and 4.2 in improving the accuracy of the ALE-SPH scheme herein adopted.

The L_2 norm of the velocity error is shown in Fig. 1(b), and the numerical values for the convergence rates θ and the norms of the velocity errors in Table 1. These results are compared with the explicit shifting formulation [27].

The convergence rate for the explicit shifting is limited to first-order, while, it reaches values higher than 2 with the IIPS. Additionally, updating the physical quantities through the advection correction step or the MLS interpolation enhances the convergence rates (also in comparison with the no-correction formulation for the IIPS algorithm) while the resolution increases.

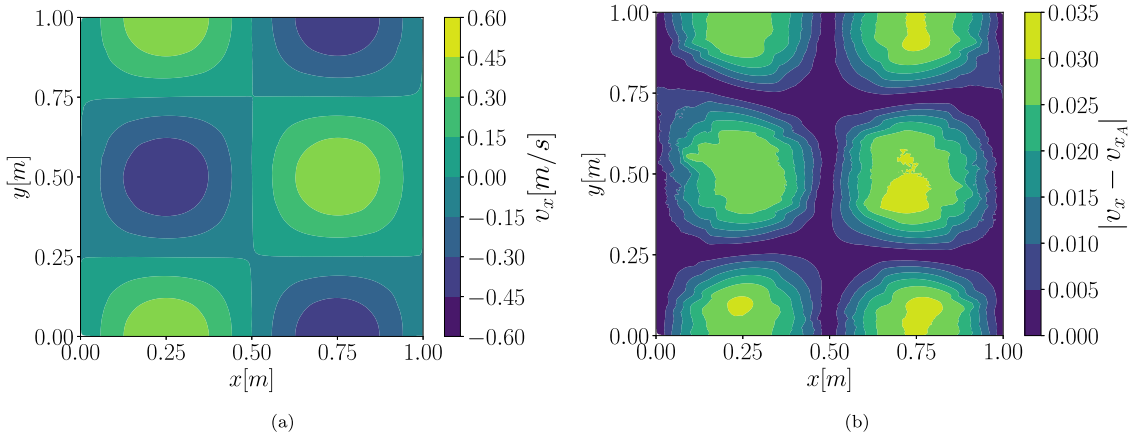

Fig. 2. TGV test case. Δ/L = 0.00625, explicit shifting [27] formulation (a) velocity x component in [m/s], (b) error on the velocity x component at physical time $t = 1$ s.

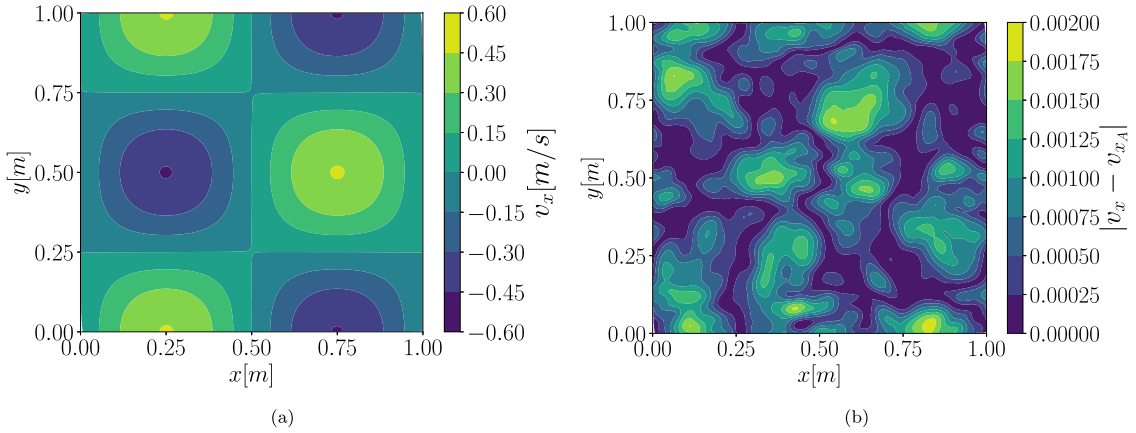

Fig. 3. TGV test case. Δ/L = 0.00625, IIPS and no correction for the physical quantities (a) velocity x component in [m/s], (b) error on the velocity x component at physical time $t = 1$ s.

The velocity field and its error are shown in Figs. 2–5, while the analysis of the error on the total kinetic energy is reported in Fig. 6; those results are referred to the higher resolution, $\Delta/L = 0.00626$. Comparing Figs. 3(b), 4(b) and 5(b) it can be noticed that the velocity field is more accurate and less noisy when the physical quantities are corrected (either by the ACS or the MLS reconstruction), this is confirmed also by the kinetic energy error shown in Fig. 6. These results confirm that for the ALE-SPH scheme herein considered, the IIPS correction produces results more accurate and with a better convergence rate than the explicit shifting formulation. Moreover, the ACS and MLS procedures adopted after the IIPS procedure significantly reduce the error of the numerical scheme in comparison with the Implicit Iterative shifting formulation without any modification of the physical quantities.

6. Applications

In the previous section, the performance of the existing approaches and the novel IIPS here proposed have been compared for a simple test case with bi-periodic boundary conditions such as the Taylor–Green flow. In this section, the focus will be posed on applications characterized by the presence of boundary conditions and free surface to

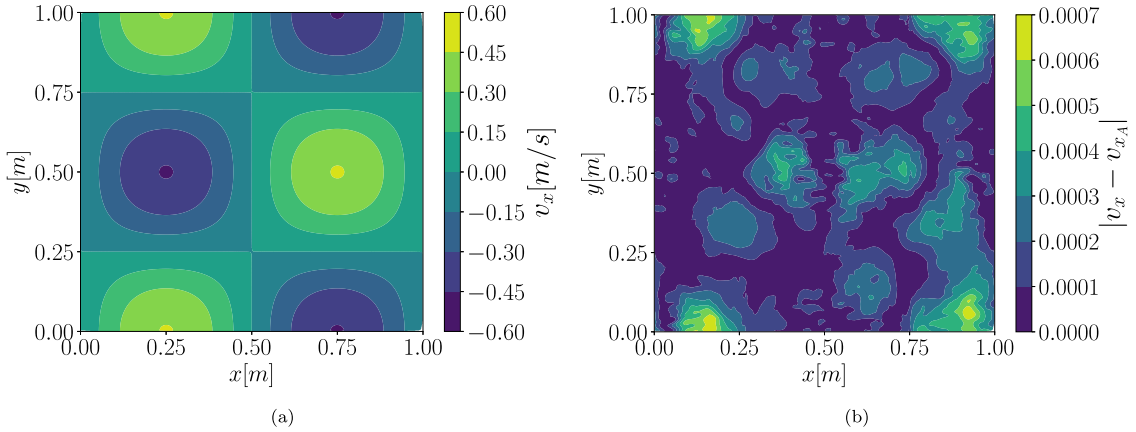

Fig. 4. TGV test case. Δ/L = 0.00625, IIPS with ACS correction for the physical quantities (a) velocity x component in [m/s], (b) error on the velocity x component at physical time $t = 1$ s.

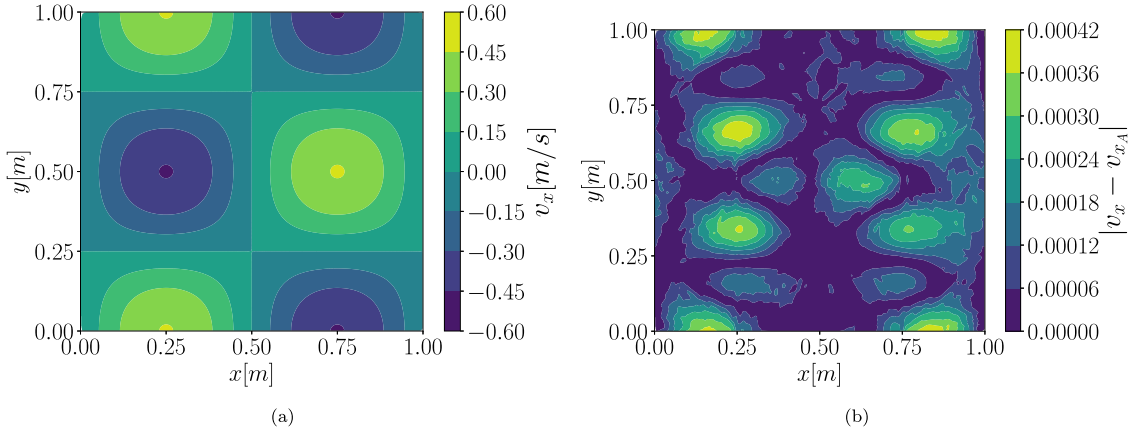

Fig. 5. TGV test case. Δ/L = 0.00625, IIPS with MLS II° correction for the physical quantities (a) velocity x component in [m/s], (b) error on the velocity x component at physical time $t = 1$ s.

further assess the accuracy and the convergence of the IIPS algorithm for improving the particle distribution in an ALE-SPH scheme.

6.1. Moving box in a rectangular domain

The flow around a moving square inside a rectangular box has been chosen to assess the IIPS algorithm in presence of moving boundary conditions as it has been identified as a benchmark test case by the SPHERIC (SPH rEsearch and engineeRing International Community) community, see for example [42,43]. The flow occurs in a rectangular box with size 10 m × 5 m, while the side of the square moving box L is 1 m and its centre of mass has initial coordinates (1.5 m, 2.5 m) as shown in Fig. 7.

The fluid is initially at rest, then the box is accelerated for 1 s until it reaches the final velocity U_{obj} = 1 m/s, which is maintained constant during the entire simulation. The reference density ρ_0 is set equal to 1000 kg/m^3 and the kinematic viscosity ν is set equal to 0.01 N/m^{2}s and therefore the Reynolds number Re is equal to 100. The reference speed of sound c_0 has been defined equal to 12 m/s in order to guarantee that the fluid can be assumed as weakly compressible. The results shown in the following section are referred to the resolution Δ/L = 0.0125.

A preliminary evaluation of the IIPS procedure has been conducted and the threshold value $L_\infty(\nabla C)_{Thr}$ to activate the IIPS procedure has been assumed equal to $0.08/h$, the test case has been performed using h/Δ = 1.2,

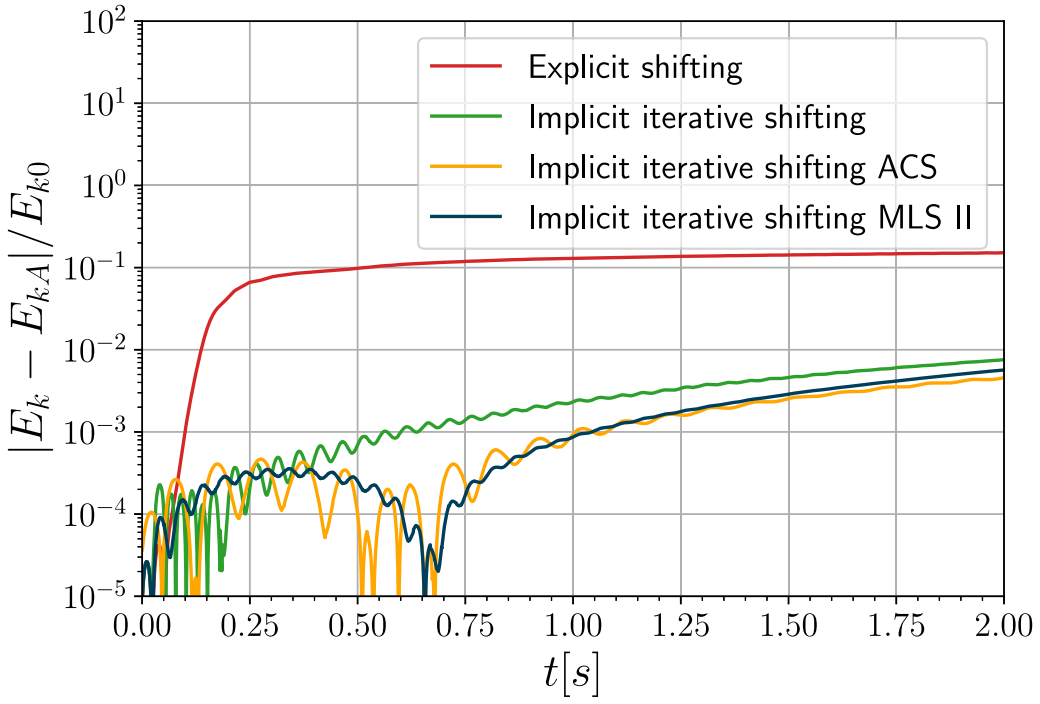

Fig. 6. TGV test case. Evolution for the Kinetic energy with resolution Δ/L = 0.00625.

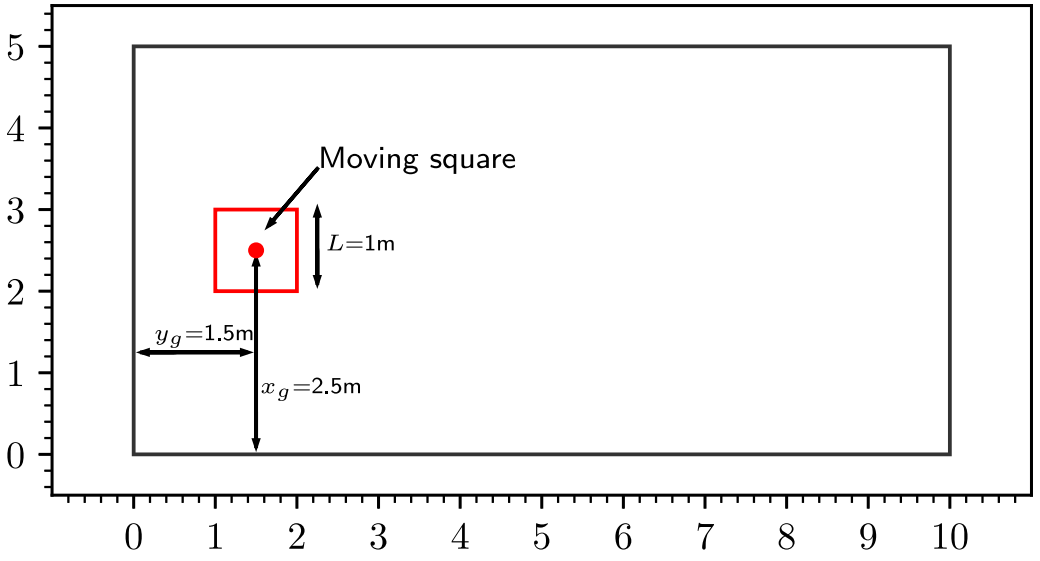

Fig. 7. Moving Box in a rectangular domain, geometry of the test case and initial location of the square.

1.5, 1.8. The maximum values of particle concentration gradient ∇C, are reported in Fig. 8, as a comparison, the results obtained using the explicit procedure are reported. It can be noted that regardless of the h/Δ ratio adopted, the prescribed maximum value of $L_\infty(\nabla C)_{Thr}$ is guaranteed by the IIPS while the original explicit shifting is not able to produce similar results.

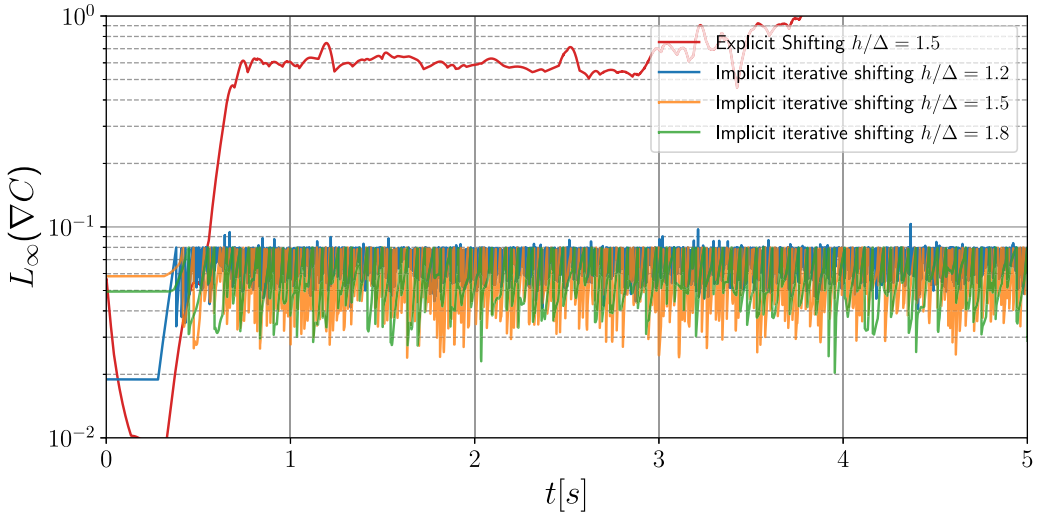

Fig. 8. Moving Box test case. Δ/L = 0.0125, $L_\infty(\nabla C)_{thr}$ = 0.08/h, h/Δ analysis.

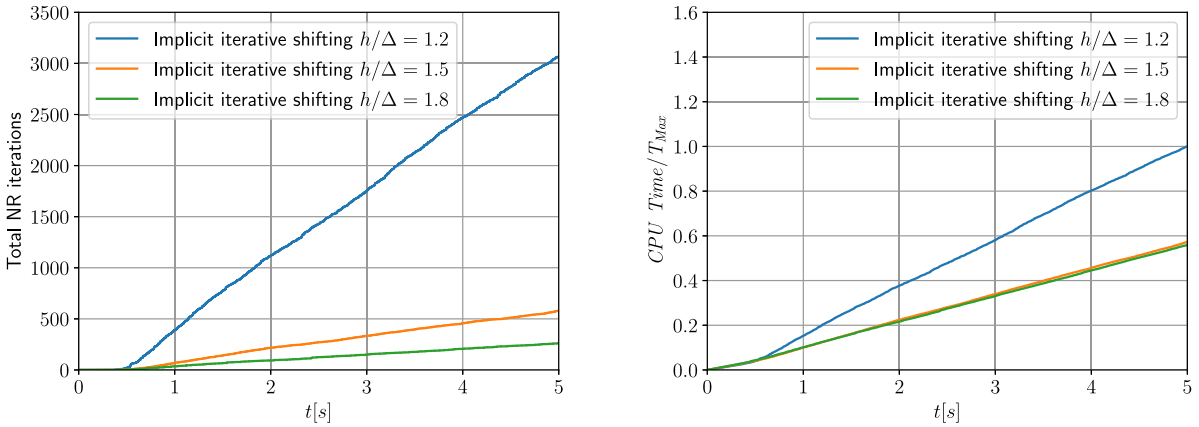

(a) Number of Newton-Raphson iterations.

(b) Normalized computational time.

Fig. 9. Moving Box test case. Δ/L = 0.0125, $L_\infty(\nabla C)_{thr}$ = 0.08/h.

Fig. 9a shows the total number of times the IIPS algorithm is activated during the simulation whereas Fig. 9b shows the non-dimensionalized total computational time of the ALE-SPH scheme considering different values of h/Δ ratio. Usually in SPH schemes, the total computational time is proportional to h/Δ ratio (as larger h/Δ correspond to an increased number of neighbours). However, in the present ALE-SPH formulation the IIPS procedure has a significant impact on the total computational time of the simulation and for smaller h/Δ ratios, the number of times the IIPS procedure is activated significantly increases (as shown in Fig. 9a). Therefore, the computational cost with h/Δ = 1.2 is about 60% higher than the one obtained with h/Δ = 1.5 or 1.8. In conclusion, it has been chosen h/Δ = 1.5, which allows keeping the predefined level of error in the particle distribution while does not increase the overall computational time.

As demonstrated by [44], the movement of the squared box generates some numerical issues, due to the highly perturbed particle distribution. Therefore, present test case has been simulated considering different particle shifting techniques and in particular: (i) explicit shifting [27], (ii) IIPS with no correction, (iii) IIPS with the advection correction step (see Eq. (17)) and (iv) IIPS with MLS reconstruction (see Section 4.2).

In Fig. 10, the ∇C field is shown at the t = 0.75 s considering the explicit shifting and the IIPS procedure. Moreover, in Fig. 11, the particle distribution near the moving square is shown at the same physical time, (when the moving square is still accelerating). It is clear that, while the explicit shifting method is not able to maintain an

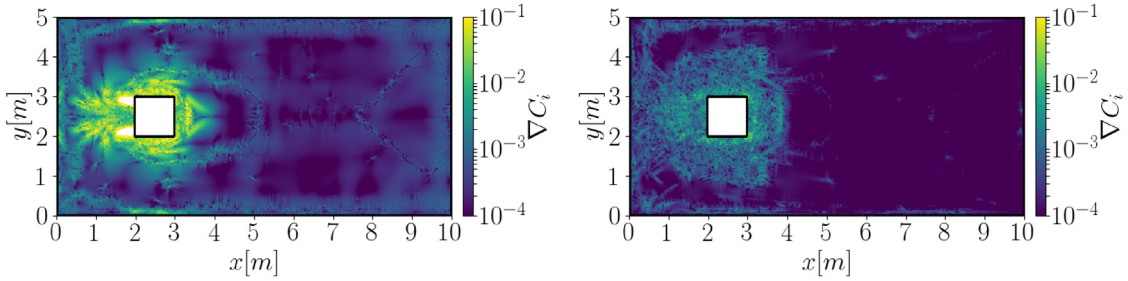

(a) Explicit shifting. (b) Implicit iterative shifting.

Fig. 10. Moving Box test case. Δ/L = 0.0125, $L_\infty(\nabla C)_{thr} = 0.08/h$. Shifting procedure comparison, particle distribution at $t = 0.75$ s.

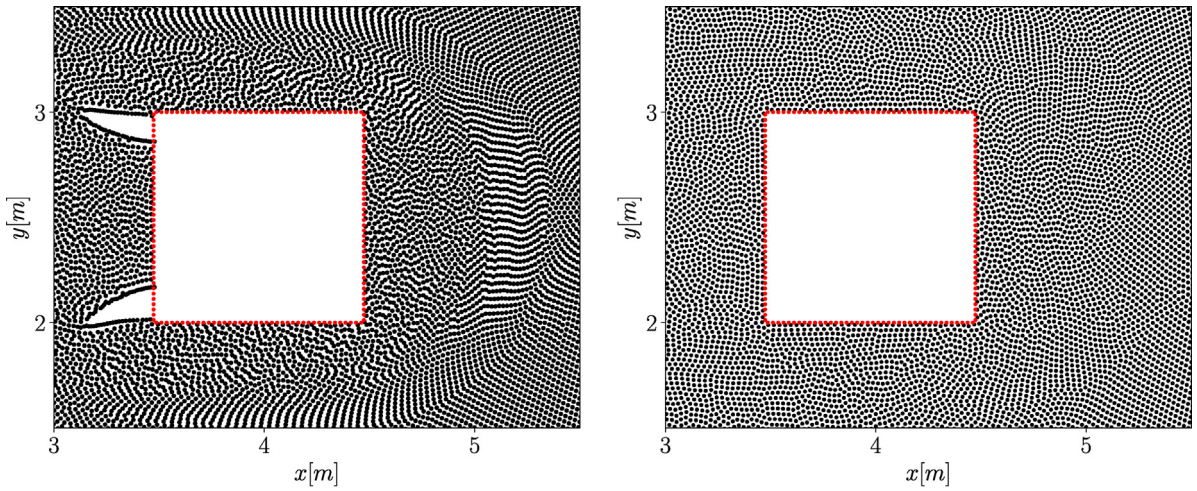

(a) Explicit shifting. (b) Implicit iterative shifting.

Fig. 11. Moving Box test case. Δ/L = 0.0125, $L_\infty(\nabla C)_{thr} = 0.08/h$. Shifting procedure comparison, particle distribution at $t = 0.75$ s.

uniform particles distribution, the IIPS procedure is capable of avoiding the formation of areas with lack of particles on the tail of the moving object.

The non-dimensional velocity fields are shown in , Fig. 12, and they can be compared with the reference solution obtained with FD solver and the SPH solution in [42].

The ALE-SPH with the IIPS, is able to produce velocity fields that are in agreement with the reference solution both using the Advection Correction Step (Fig. 12a), and the second-order MLS interpolation (Fig. 12b). The velocity in the wake of the moving square shown in Fig. 12b is slightly underestimated, and this is due to the additional numerical dissipation of the MLS algorithm. The normalized total computational times have been monitored and the results are shown in Fig. 13. The ranges of computational overhead are similar to the ones obtained in the theoretical test case in Section 5: the ACS and the MLS interpolation increase the CPU time respectively by 33 and by 54 percent in comparison with the explicit shifting formulation. In this test case, the presence of a moving square and external walls act as constraints on the rearrangement of particles. The IIPS performances are superior with respect to the explicit shifting methodology both in terms of quality of the particle distribution and in terms of final results (velocity magnitude maps). Moreover, the computational times are not drastically increased and remain affordable.

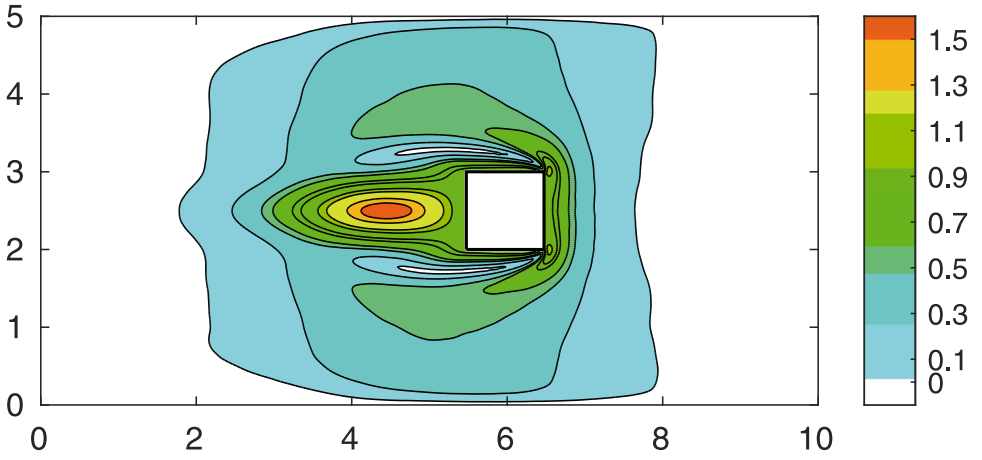

(a) IISP with Advection Correction Step

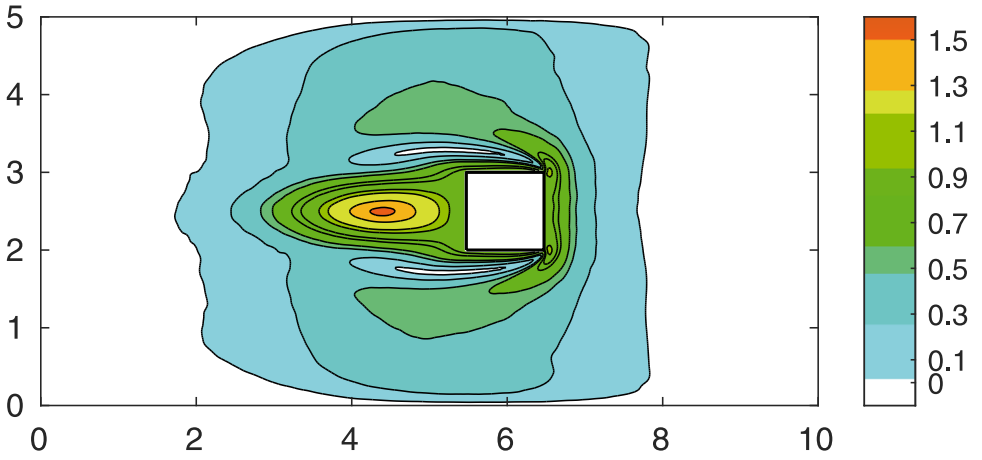

(b) IISP with Moving Least Square reinterpolation

Fig. 12. Moving Box test case. Non-dimensional velocity field $\boldsymbol{v}/U_{ref}$. $\Delta/L = 0.0125$, $L_\infty(\nabla C)_{thr} = 0.08/h$, $Re = 100$ at $t = 5$ s.

6.2. Impinging jet on a flat surface

In this section an impinging jet on a flat surface has been simulated with the aim of assessing the capability of the proposed numerical scheme in presence of free surface. For this test case Taylor [45] derived the following implicit solution for velocity and pressure at the wall, with an arbitrary degree of impact:

$$\begin{cases} \dfrac{x}{H} = & \dfrac{1}{2}(1+\cos\varphi)\ln\left(\dfrac{1+q}{1-q}\right) + \sin\varphi \sin q^{-1} \\ u = & \dfrac{\sqrt{(1-q^2)\sin\varphi} - 1 - \cos\varphi}{q - \cos\varphi} \\ p = & \dfrac{1}{2}\rho U^2\left(1-u^2\right) \end{cases} \tag{20}$$

where q is a free parameter in the solution, φ is the angle measured from the vertical (90° in this case), x is the horizontal distance from the stagnation point, H is the half-width of the inflow section, and U is the jet velocity. The test case has been simulated with resolutions equal to $H/\Delta = 10$, $H/\Delta = 20$ and $H/\Delta = 40$. The inflow velocity is $U = 100$ m/s, the reference speed of sound is set $c_0 = 1000$ m/s, in order to guarantee that the fluid can be assumed as weakly compressible. To deal with free-surface flows particles with ∇C lower than a threshold value

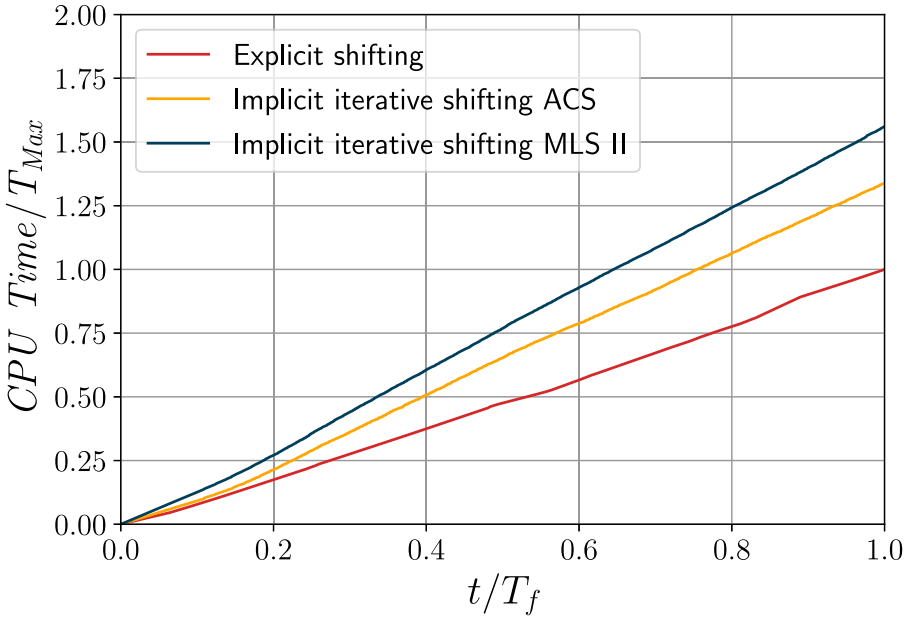

Fig. 13. Moving Box test case. $\Delta/L = 0.0125$, Shifting procedure comparison, CPU time.

are identified as free-surface particles and their position is frozen when the IIPS algorithm is activated, and those particles maintain a pure Lagrangian motion. This is obtained by removing the free-surface particles from the linear system of Eqs. (9) and (10), of the IIPS procedure. Therefore, the size of the adjusted linear system downgrades to $d \cdot (n - n_{int})$, where d is the number of dimensions, n the number of fluid particles and n_{int} is the number of the free-surface particles; in this way the implicit corrections are applied to interior fluid particles only.

To assess the value of $L_\infty(\nabla C)_{thr}$, which has to be imposed during the physical simulations, an initial investigation on the particles distribution has been conducted, using $H/\Delta = 10$. Fig. 14 shows the $L_\infty(\nabla C)$, computed in the region of the domain defined as $x/L = [-0.3, 0.3]$ and $z/L = [0, 0.6]$, using both the explicit shifting and IIPS procedures activated at each time step, regardless to the maximum ∇C value. The maximum values of $L_\infty(\nabla C)$ obtained by the IIPS procedure is about two orders of magnitude smaller than the one produced by the explicit shifting, confirming that the IIPS is guaranteeing an homogeneous particle distribution.

The particle concentration gradient ∇C, is shown in Figs. 15 and 16, at $tU/L = 0.0525$ using the explicit shifting and the IIPS procedure, respectively. Following this preliminary analysis it has been possible to set the threshold to activate the IIPS algorithm $L_\infty(\nabla C)_{thr}$ equal to $0.02/h$ that is used in the remainder of the section. As for previous test cases, the IIPS procedure is able to keep the ∇C below the predefined threshold $L_\infty(\nabla C)$ for all particles during the entire simulation as shown in Fig. 17.

As previously mentioned, the pressure at the stagnation point and along the flat surface has been compared with the analytical solution of Eq. (20), considering the explicit shifting (Fig. 18), IIPS with the advection correction step (Fig. 19) and IIP with the MLS reconstruction (Fig. 20). Please note that, whereas the pressure at the stagnation point is plotted against time, the pressure along the flat surface has been obtained by averaging the values in the normalized time interval $tU/L = [2, 3]$. The numerical values for pressure along the flat surface and the percentage errors are reported in Table 2. It can be seen that the original explicit shifting formulation has a percentage error higher than 10%, close to the stagnation point. Differently, both IIPS algorithms drastically reduce the pressure error along the plate: the percentage error of $P(0)/\rho U^2$, (which corresponds to the point of higher perturbation of the Lagrangian streamlines), using the ACS and the MLS interpolation are respectively 2.85% and 1.45% with respect to the analytical value. In Figs. 18(b), 19(b) and 20(b) the pressure at the stagnation point P_0 is plotted against time. The highly distorted particle distribution generated by the explicit shifting generates underestimated values. On the contrary, the IIPS formulations are more accurate. Additionally, it is worth to be noted that even reducing the particle size, the explicit shifting is not able to increase accuracy in the area close to the stagnation point, while

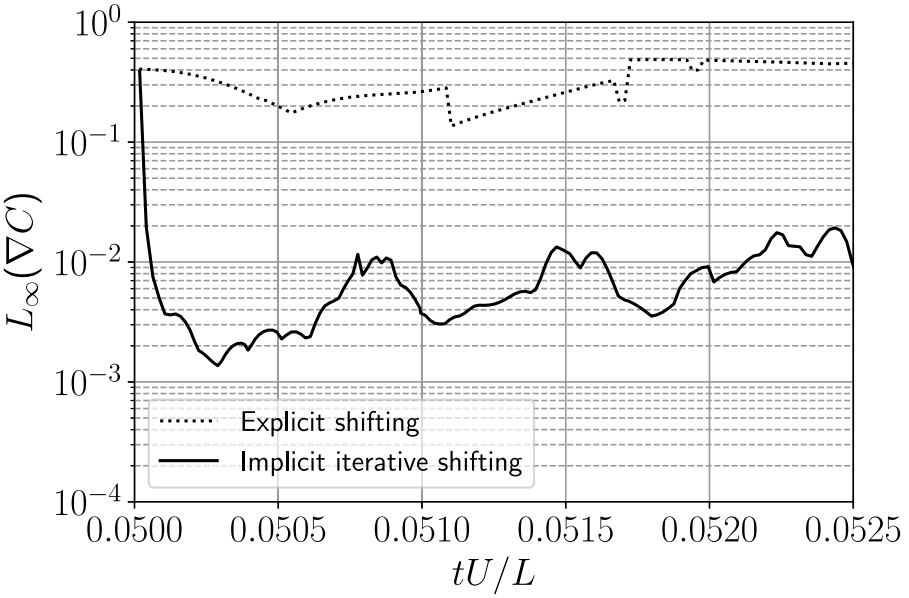

Fig. 14. Impinging Jet test case. $H/\Delta = 10$, Shifting procedure comparison with IIPS activated at each timestep.

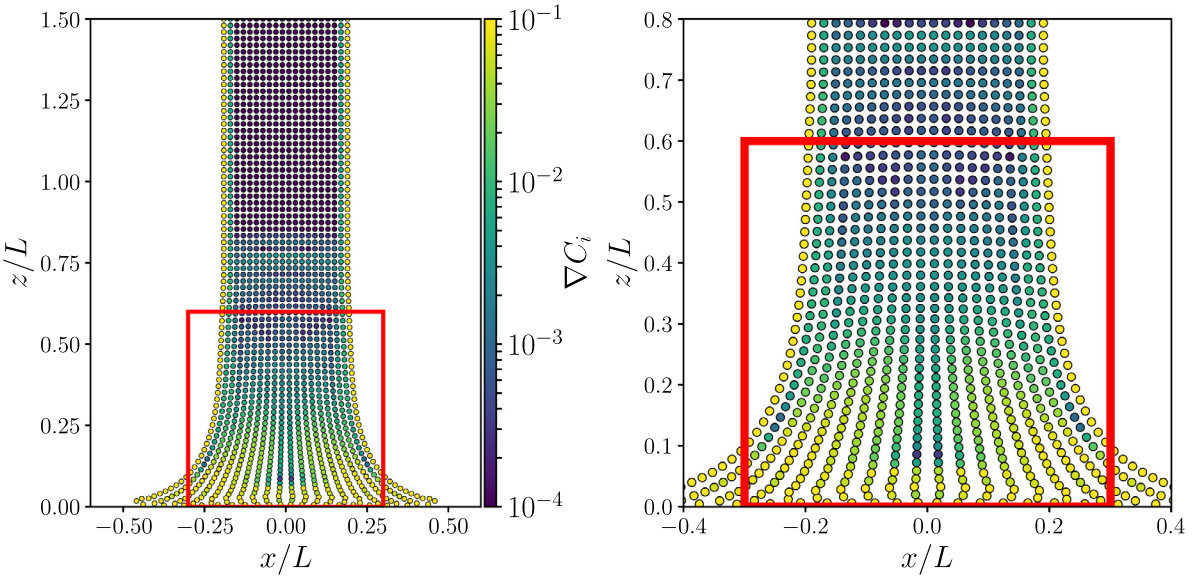

Fig. 15. Impinging Jet test case. $H/\Delta = 10$, ∇C, explicit shifting, at $tU/L = 0.0525$.

simulations with IIPS procedure generate converging results. The errors obtained using the MLS reinterpolation are lower at the stagnation point compared to the advection procedure but of the same order of magnitude. In Fig. 21 the normalized computational time is reported and it is verified that the CPU time is not drastically increased. Please note that, in both the APS and MLS interpolation the most expensive part of the algorithm is the IIPS procedure for computing the new particle position by solving the linear system of Eqs. (9) and (10) .

7. Conclusion

In the present work, two different strategies to embed the Implicit Iterative Particle Shifting formulation in an SPH-ALE solver have been proposed. These methodologies have been called Implicit iterative shifting with

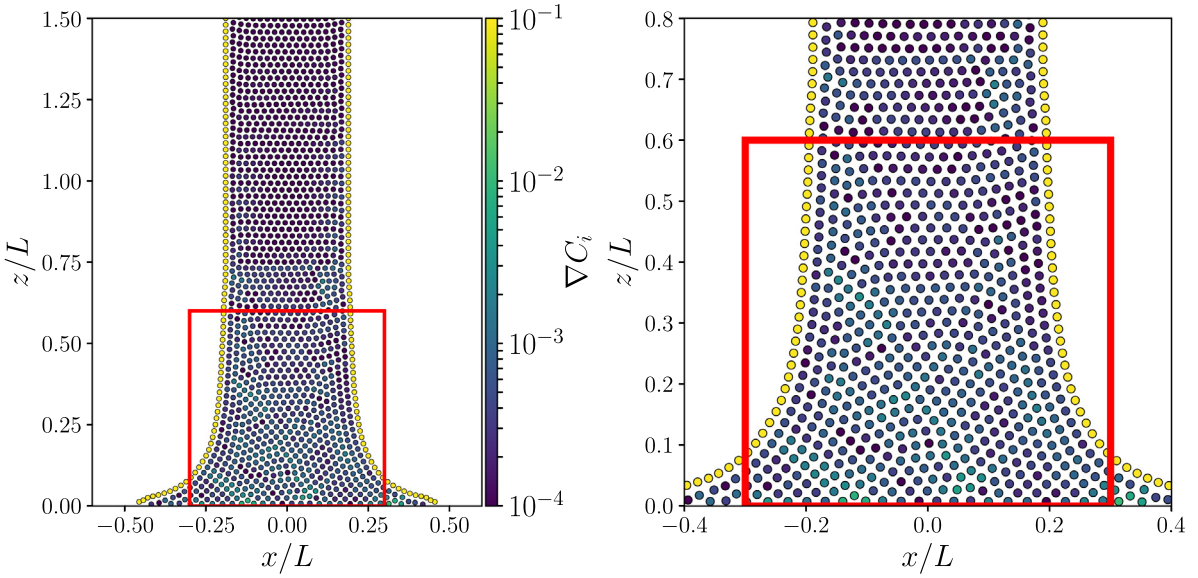

Fig. 16. Impinging Jet test case. $H/\Delta = 10$, ∇C, implicit iterative shifting at $tU/L = 0.0525$.

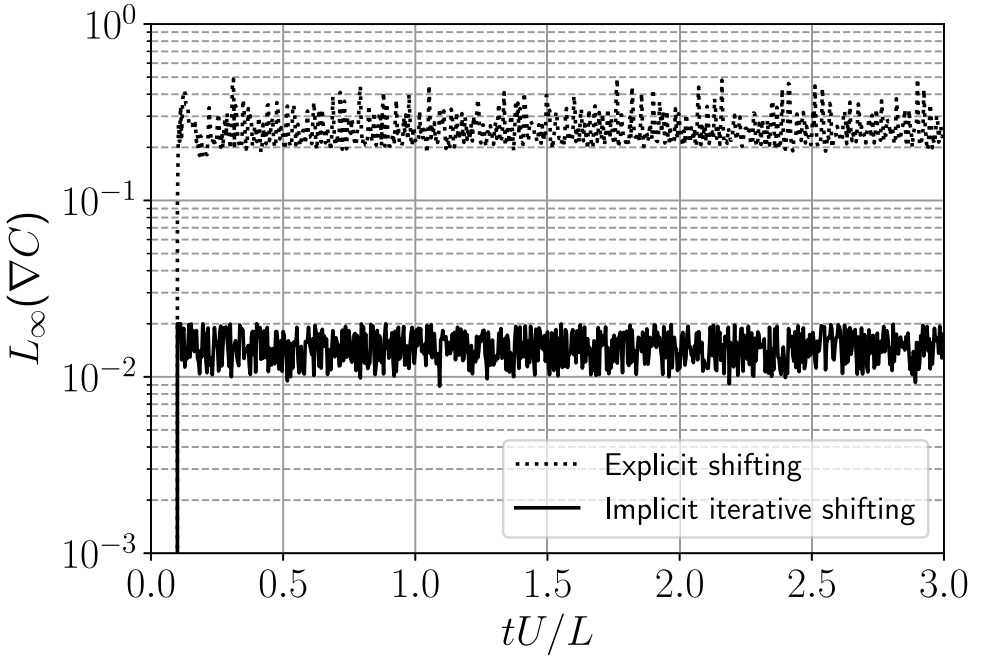

Fig. 17. Impinging Jet test case. $H/\Delta = 10$, Shifting procedure comparison with $L_\infty(\nabla C)_{thr}$ equal to $0.02/h$.

Advection Correction Step and Implicit iterative shifting with MLS interpolation, both of them have been introduced to update the physical quantities at the end of the implicit procedure allowing to maintain consistency in the numerical scheme. To adjust volume, mass and momentum on the particle distribution obtained using the IIPS, the first one adopts the ALE formalism to compute the convective fluxes generated by the implicit shifting displacements, while the second one makes a pure geometric interpolation using the information of the original particle distribution. Two different applications, which are representative of a wide range of practical problems, have been simulated using the shifting methodologies introduced in this project demonstrating that the implicit

Table 2
Impinging Jet test case. Δ/L = 0.0005. Normalized average pressure on the plate and percentage error $E_{r\%}$.

x/L	Explicit		IIPS-ACS		IIPS-MLS II	
	$P/\rho U^2$	$E_{r\%}$	$P/\rho U^2$	$E_{r\%}$	$P/\rho U^2$	$E_{r\%}$
0.0	0.448	10.48	0.486	2.85	0.493	1.45
−0.05	0.444	10.38	0.481	2.88	0.487	1.62
−0.10	0.432	10.37	0.466	3.18	0.473	1.84
−0.15	0.412	10.25	0.441	3.73	0.448	2.24
−0.20	0.384	9.80	0.408	4.16	0.414	2.74
−0.25	0.351	8.82	0.368	4.36	0.373	3.13
−0.30	0.309	7.84	0.320	4.49	0.324	3.19
−0.35	0.263	6.17	0.269	3.81	0.273	2.69
−0.40	0.216	3.43	0.218	2.26	0.221	1.16

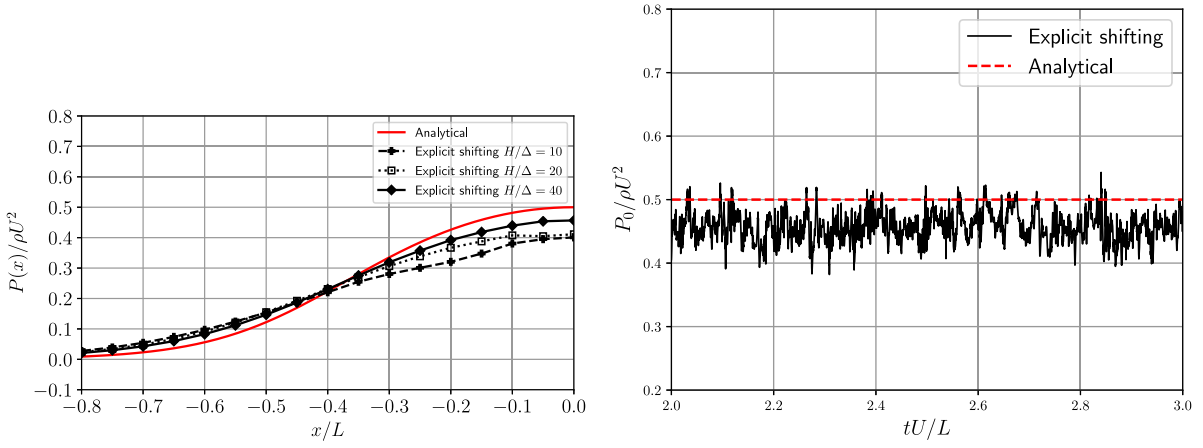

(a) Normalized pressure (b) Normalized pressure

Fig. 18. Impinging Jet test case explicit shifing. Δ/L = 0.001, shifting procedure comparison, normalized pressure at P_0 in the time interval $tU/L = [2, 3]$.

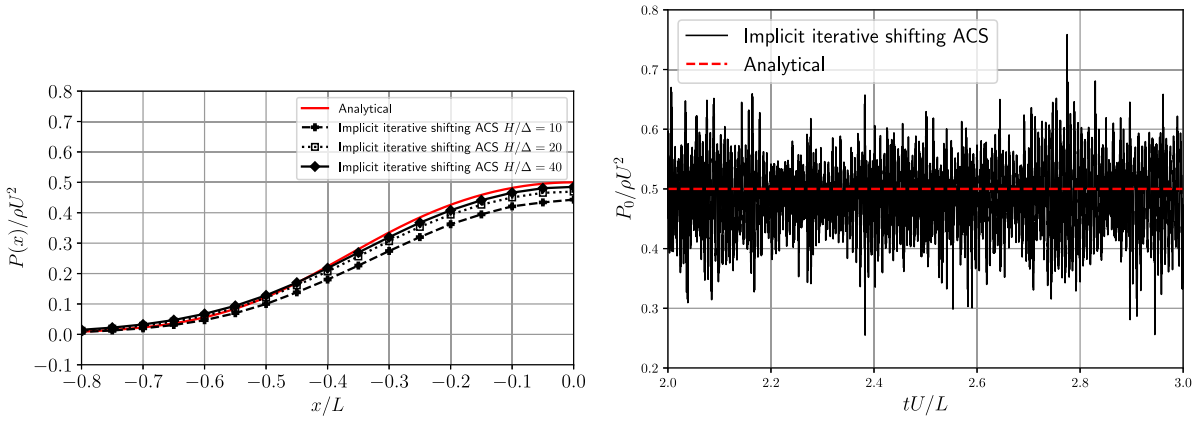

(a) Normalized pressure (b) Normalized pressure

Fig. 19. Impinging Jet test case advection correction step. Δ/L = 0.001, shifting procedure comparison, normalized pressure at P_0 in the time interval $tU/L = [2, 3]$.

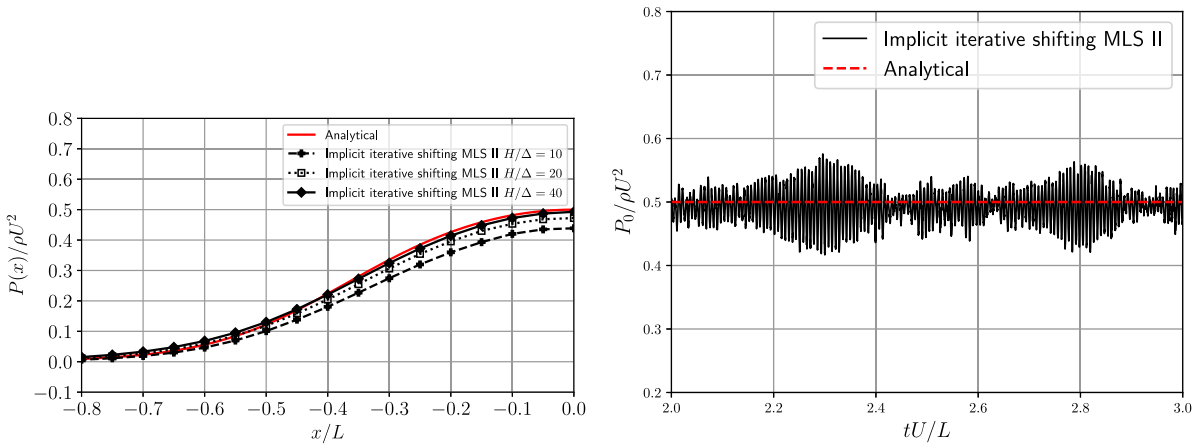

(a) Normalized pressure (b) Normalized pressure

Fig. 20. Impinging Jet test case. MLS reinterpolation. Δ/L = 0.001, shifting procedure comparison, normalized pressure at P_0 in the time interval $tU/L = [2, 3]$.

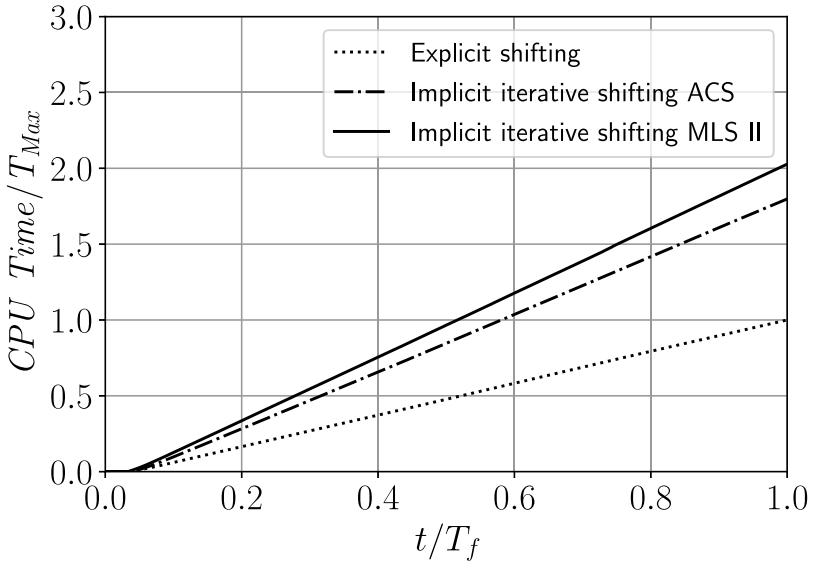

Fig. 21. Impinging Jet test case. Δ/L = 0.0125, Shifting procedure comparison, CPU time.

iterative methodology has superior performance in controlling the particle distribution quality and in maintaining a predefined level of discretization error of the SPH interpolation. Moreover both the ACS and the MLS interpolation are able to improve the quality of the results with respect to the IIPS approach without any correction for the physical quantities. The former formulation guarantees the conservation of the physical quantities whereas the latter improves the quality of the pressure field in presence of strong impacts such as in the impinging jet on a flat surface.

Declaration of competing interest

The authors declare that they have no known competing financial interests or personal relationships that could have appeared to influence the work reported in this paper.

Data availability

No data was used for the research described in the article.

References

[1] R.A. Gingold, J.J. Monaghan, Smoothed particle hydrodynamics: theory and application to non-spherical stars, Mon. Not. R. Astron. Soc. 181 (3) (1977) 375–389.

[2] L.B. Lucy, A numerical approach to the testing of the fission hypothesis, Astron. J. 82 (1977) 1013–1024.

[3] J.J. Monaghan, Smoothed particle hydrodynamics, Annu. Rev. Astron. Astrophys. 30 (1) (1992) 543–574.

[4] J.J. Monaghan, Smoothed particle hydrodynamics and its diverse applications, Annu. Rev. Fluid Mech. 44 (2012) 323–346.

[5] J.J. Monaghan, Simulating free surface flows with SPH, J. Comput. Phys. 110 (2) (1994) 399–406.

[6] M. Gomez-Gesteira, B.D. Rogers, R.A. Dalrymple, A.J. Crespo, State-of-the-art of classical SPH for free-surface flows, J. Hydraul. Res. 48 (sup1) (2010) 6–27.

[7] J.M. Domínguez, G. Fourtakas, C. Altomare, R.B. Canelas, A. Tafuni, O. García-Feal, I. Martínez-Estévez, A. Mokos, R. Vacondio, A.J. Crespo, et al., DualSPHysics: From fluid dynamics to multiphysics problems, Comput. Part. Mech. 9 (5) (2022) 867–895.

[8] S. Shao, SPH simulation of solitary wave interaction with a curtain-type breakwater, J. Hydraul. Res. 43 (4) (2005) 366–375.

[9] B.D. Rogers, R.A. Dalrymple, SPH modeling of tsunami waves, in: Advanced Numerical Models for Simulating Tsunami Waves and Runup, World Scientific, 2008, pp. 75–100.

[10] J. O'Connor, B.D. Rogers, A fluid–structure interaction model for free-surface flows and flexible structures using smoothed particle hydrodynamics on a GPU, J. Fluids Struct. (ISSN: 0889-9746) 104 (2021) 103312, http://dx.doi.org/10.1016/j.jfluidstructs.2021.103312, URL https://www.sciencedirect.com/science/article/pii/S0889974621000955.

[11] A. Colagrossi, M. Landrini, Numerical simulation of interfacial flows by smoothed particle hydrodynamics, J. Comput. Phys. 191 (2) (2003) 448–475.

[12] S. Adami, X. Hu, N.A. Adams, A transport-velocity formulation for smoothed particle hydrodynamics, J. Comput. Phys. 241 (2013) 292–307.

[13] G. Fourtakas, B. Rogers, Modelling multi-phase liquid-sediment scour and resuspension induced by rapid flows using Smoothed Particle Hydrodynamics (SPH) accelerated with a Graphics Processing Unit (GPU), Adv. Water Resour. (ISSN: 0309-1708) 92 (2016) 186–199, http://dx.doi.org/10.1016/j.advwatres.2016.04.009, URL https://www.sciencedirect.com/science/article/pii/S0309170816300926.

[14] N.J. Quinlan, M. Basa, M. Lastiwka, Truncation error in mesh-free particle methods, Internat. J. Numer. Methods Engrg. 66 (13) (2006) 2064–2085.

[15] J. Monaghan, On the problem of penetration in particle methods, J. Comput. Phys. 82 (1989) 1–15.

[16] A. Chaniotis, D. Poulikakos, P. Koumoutsakos, Remeshed smoothed particle hydrodynamics for the simulation of viscous and heat conducting flows, J. Comput. Phys. 182 (1) (2002) 67–90.

[17] R. Nestor, N. Quinlan, Extension of the finite volume particle method to higher order accuracy and viscous flow, in: SPHERIC-Smoothed Particle Hydrodynamics European Research Interest Community, 2007, p. 95.

[18] R. Xu, P. Stansby, D. Laurence, Accuracy and stability in incompressible SPH (ISPH) based on the projection method and a new approach, J. Comput. Phys. 228 (18) (2009) 6703–6725.

[19] S. Lind, R. Xu, P. Stansby, B.D. Rogers, Incompressible smoothed particle hydrodynamics for free-surface flows: A generalised diffusion-based algorithm for stability and validations for impulsive flows and propagating waves, J. Comput. Phys. 231 (4) (2012) 1499–1523.

[20] A. Skillen, S. Lind, P.K. Stansby, B.D. Rogers, Incompressible smoothed particle hydrodynamics (SPH) with reduced temporal noise and generalised Fickian smoothing applied to body–water slam and efficient wave–body interaction, Comput. Methods Appl. Mech. Engrg. (ISSN: 0045-7825) 265 (2013) 163–173, http://dx.doi.org/10.1016/j.cma.2013.05.017.

[21] M.S. Shadloo, A. Zainali, M. Yildiz, A. Suleman, A robust weakly compressible SPH method and its comparison with an incompressible SPH, Internat. J. Numer. Methods Engrg. 89 (8) (2012) 939–956.

[22] R. Vacondio, B. Rogers, P.K. Stansby, P. Mignosa, J. Feldman, Variable resolution for SPH: a dynamic particle coalescing and splitting scheme, Comput. Methods Appl. Mech. Engrg. 256 (2013) 132–148.

[23] R. Vacondio, B. Rogers, Consistent iterative shifting for SPH methods, in: Proceedings of 12th International SPHERIC Workshop, Ourense, Spain, 2017.

[24] P. Sun, A. Colagrossi, S. Marrone, M. Antuono, A.-M. Zhang, A consistent approach to particle shifting in the δ-Plus-SPH model, Comput. Methods Appl. Mech. Engrg. 348 (2019) 912–934.

[25] J. Vila, On particle weighted methods and smooth particle hydrodynamics, Math. Models Methods Appl. Sci. 9 (02) (1999) 161–209.

[26] G. Oger, S. Marrone, D. Le Touzé, M. De Leffe, SPH accuracy improvement through the combination of a quasi-Lagrangian shifting transport velocity and consistent ALE formalisms, J. Comput. Phys. 313 (2016) 76–98.

[27] M. Neuhauser, Development of a Coupled SPH-ALE/Finite Volume Method for the Simulation of Transient Flows in Hydraulic Machines (Ph.D. thesis), Ecully, Ecole centrale de Lyon, 2014.

[28] M. Antuono, A. Colagrossi, S. Marrone, Numerical diffusive terms in weakly-compressible SPH schemes, Comput. Phys. Comm. 183 (12) (2012) 2570–2580.

[29] J. Michel, A. Vergnaud, G. Oger, C. Hermange, D. Le Touzé, On Particle Shifting Techniques (PSTs): Analysis of existing laws and proposition of a convergent and multi-invariant law, J. Comput. Phys. (2022) 110999.

[30] P. Rastelli, R. Vacondio, J. Marongiu, G. Fourtakas, B.D. Rogers, Implicit iterative particle shifting for meshless numerical schemes using kernel basis functions, Comput. Methods Appl. Mech. Engrg. 393 (2022) 114716.

[31] J.-C. Marongiu, Méthode Numérique Lagrangienne Pour La Simulation D'écoulements À Surface Libre: Application Aux Turbines Pelton (Ph.D. thesis), Ecully, Ecole centrale de Lyon, 2007.

[32] S.F. Pineda Rondon, Numerical Prediction of Cavitation Erosion (Ph.D. thesis), Lyon, 2017.

[33] C.W. Hirt, A.A. Amsden, J. Cook, An arbitrary Lagrangian-Eulerian computing method for all flow speeds, J. Comput. Phys. 14 (3) (1974) 227–253.
[34] J. Leduc, Etude Physique Et Numérique De L'écoulement Dans Un Systeme D'injection De Turbine Pelton (Ph.D. thesis), Thèse De Doctorat, Ecole Centrale De Lyon, 2010.
[35] B. Van Leer, Towards the ultimate conservative difference scheme. V. A second-order sequel to Godunov's method, J. Comput. Phys. 32 (1) (1979) 101–136.
[36] C. Hirsch, Numerical Computation of Internal and External Flows: The Fundamentals of Computational Fluid Dynamics, Elsevier, 2007.
[37] R. Vacondio, C. Altomare, M. Dea Leffe, X. Hu, D. Lea Touzé, S. Lind, J.-C. Marongiu, S. Marrone, B.D. Rogers, A. Souto-Iglesias, Grand challenges for Smoothed Particle Hydrodynamics numerical schemes, Comput. Part. Mech. (2020) 1–14, Springer.
[38] A. Amicarelli, J.-C. Marongiu, F. Leboeuf, J. Leduc, J. Caro, SPH truncation error in estimating a 3D function, Comput. & Fluids 44 (1) (2011) 279–296.
[39] P. Sun, A. Colagrossi, S. Marrone, A. Zhang, The δplus-SPH model: Simple procedures for a further improvement of the SPH scheme, Comput. Methods Appl. Mech. Engrg. 315 (2017) 25–49.
[40] M. Antuono, P. Sun, S. Marrone, A. Colagrossi, The δ -ALE-SPH model: An arbitrary Lagrangian-Eulerian framework for the δ -SPH model with particle shifting technique, Comput. & Fluids (ISSN: 0045-7930) 216 (2021) 104806, http://dx.doi.org/10.1016/j.compfluid.2020.104806, URL https://www.sciencedirect.com/science/article/pii/S0045793020303765.
[41] G.-A. Renaut, Schémas D'ordre Élevé Pour La Méthode SPH-ALE Appliquée À Des Simulations Sur Machines Hydrauliques (Ph.D. thesis), Ecully, Ecole centrale de Lyon, 2015.
[42] G. Colicchio, M. Greco, O. Faltinsen, Fluid-body interaction on a Cartesian grid: dedicated studies for a CFD validation, in: Proc. IWWWFB, Vol. 6, 2006.
[43] S. Marrone, A. Colagrossi, M. Antuono, G. Colicchio, G. Graziani, An accurate SPH modeling of viscous flows around bodies at low and moderate Reynolds numbers, J. Comput. Phys. (ISSN: 0021-9991) 245 (2013) 456–475, http://dx.doi.org/10.1016/j.jcp.2013.03.011, URL https://www.sciencedirect.com/science/article/pii/S0021999113001885.
[44] E.-S. Lee, Truly Incompressible Approach for Computing Incompressible Flow in SPH and Comparisons with the Traditional Weakly Compressible Approach, The University of Manchester (United Kingdom), 2007.
[45] G. Taylor, Oblique impact of a jet on a plane surface, Phil. Trans. R. Soc. 260 (1110) (1966) 96–100, cited By 47.